Nanoscale

COMMUNICATION

View Article Online
View Journal | View Issue

Nano-sensitive optical coherence tomography†

Cite this: *Nanoscale*, 2014, **6**, 3545

Sergey A. Alexandrov,* Hrebesh M. Subhash, Azhar Zam and Martin Leahy

Received 18th November 2013
Accepted 16th January 2014

DOI: 10.1039/c3nr06132a

www.rsc.org/nanoscale

Depth resolved label-free detection of structural changes with nanoscale sensitivity is an outstanding problem in the biological and physical sciences and has significant applications in both the fundamental research and healthcare diagnostics arenas. Here we experimentally demonstrate a novel label-free depth resolved sensing technique based on optical coherence tomography (OCT) to detect structural changes at the nanoscale. Structural components of the 3D object, spectrally encoded in the remitted light, are transformed from the Fourier domain into each voxel of the 3D OCT image without compromising sensitivity. Spatial distribution of the nanoscale structural changes in the depth direction is visualized in just a single OCT scan. This label free approach provides new possibilities for depth resolved study of pathogenic and physiologically relevant molecules in the body with high sensitivity and specificity. It offers a powerful opportunity for early diagnosis and treatment of diseases. Experimental results show the ability of the approach to differentiate structural changes of 30 nm in nanosphere aggregates, located at different depths, from a single OCT scan, and structural changes less than 30 nm in time from two OCT scans. Application for visualization of the structure of human skin *in vivo* is also demonstrated.

Most of the fundamental pathological processes in living tissues, including cancer, exhibit changes at the nanolevel. Recently the diffraction resolution limit has been broken and optical nanoscale microscopy has led to the creation of nanoscopic medicine. However, nanoscopy largely requires labelling, is limited to superficial 2D imaging and is not suitable for *in vivo* applications.[1–3] Furthermore, it is becoming more obvious that 2D biology often does not translate into the real 3D situation.

A spectral encoding of spatial frequency (SESF) approach for quantitative characterization of the structure with nanoscale sensitivity has been developed recently.[4–6] The ability to map axial structural information, profile of the axial spatial periods, into each pixel of a 2D image with nanoscale sensitivity has been demonstrated[4,5] and the application of this approach to 3D microscopic imaging has been theoretically postulated.[6]

Optical coherence tomography (OCT), an optical analogue of ultrasound techniques, provides non-invasive, contactless depth resolving *in vivo* imaging of the object's internal structure.[7] OCT has recently begun to revolutionize medical diagnostics. It is the fastest growing medical imaging modality, with annual re-imbursement for ophthalmic assessments exceeding $1Bln and the systems market exceeding $400M from virtually nothing a decade earlier. OCT facilitates cellular level structural and functional imaging of living animal and human tissues, but the structural sensitivity and resolution are fundamentally limited to the microscale.[8–10]

New approaches to improve the information content provided by OCT have been developed. Light scattering spectroscopy (LSS) was incorporated in OCT for depth resolved nuclear morphology measurements.[11,12] Spectroscopic information was extracted from OCT data,[13] angular resolved low coherence interferometry was demonstrated for the assessment of subcellular features,[14] and molecular imaging was realized.[15] Interferometric synthetic aperture microscopy (ISAM) has been developed to improve the out of focal plane resolution.[16] Recently the application of phase sensitive OCT to vibration measurements in the hearing organs,[17] including in a contribution from a co-author of this paper,[18] and for investigation of the human retina[19] at the nanoscale has been demonstrated.

NBIPI Tissue Optics & Microcirculation Imaging Group, School of Physics, National University of Ireland, Galway, Ireland. E-mail: sergey.alexandrov@nuigalway.ie

† Electronic supplementary information (ESI) available: Theory of the nsOCT. Figure: axial spatial period profiles for two selected points within the sample for second and fiftieth frames and averaged over all frames before (0 nm) and after (30 nm) nanoscale structural changes. Videos 1 and 2: axial spatial period profiles for selected points within tubes with intralipid *versus* time where fast structural changes can be seen. Videos 3 and 4: axial spatial period profiles for selected points outside from tubes with intralipid *versus* time where slow structural changes can be seen. Video 5: nsOCT imaging of the structural changes within tubes with intralipid. Videos 6 and 8: axial spatial period profiles for selected points within human fingertip *versus* time where slow structural changes can be seen. Videos 7 and 9: axial spatial period profiles for selected points within human fingertip *versus* time where fast structural changes can be seen. Video 10: nsOCT imaging of the structural changes within human fingertip *in vivo*. See DOI: 10.1039/c3nr06132a

The ability of OCT to sense nanoscale structural alterations in weakly scattering media has been discussed.[20]

In spite of the fact that the ability of existing approaches to probe structures at micro- and nanoscale has been shown, the depth resolved probing of the 3D structure of scattering objects with nanoscale sensitivity using just a single OCT scan remains a problem. In this Communication we demonstrate that the SESF approach can be adapted to OCT and introduce nano-sensitive OCT (nsOCT).

A solution of the optical inverse scattering problem was presented by Wolf.[21,22] It was shown that 3D scattering potential of the object can be reconstructed from the distribution of complex amplitudes of the light scattered by the object in the far zone (complex amplitudes of spatial frequencies) *via* 3D Fourier transform. One possible way to obtain these complex amplitudes of the spatial frequencies is multi-wavelength illumination. Fourier domain OCT is based on a modification of the original formalism for the one-dimensional problem.[23] The range of axial spatial frequencies in OCT is limited by spectral bandwidth of the light source and the resolution of spatial frequencies is limited by spectral resolution. It is known that the axial Fourier spectrum of the object is very informative and highly sensitive to structural changes.[6] In conventional OCT, during the inverse Fourier transform to reconstruct the axial profile, the spatial information is integrated and, as a result, reduces the resolution and sensitivity of the OCT. Following the SESF approach, with the information about both 3D *K*-space and reconstructed object space, we can perform structural characterization for a given volume of interest within the object with nanoscale sensitivity using a simple method utilizing the characteristics of the spatial frequency support in *K*-space. In nsOCT for each A-scan (one axial scan along the depth direction) only information about 1D *K*-space and the corresponding depth profile is presented. Given that wavelength is spatially invariant (is not changed when translated from *K*-space to image space), by encoding each axial spatial frequency (or period) with one unique wavelength, the spectrally encoded axial spatial period can be carried from the *K*-space to the reconstructed object space without compromising accuracy. By mapping the energy contribution of the spectrally encoded axial spatial period to each voxel within the 3D OCT image, we are able to perform structural characterization of every volume of interest of the object with nanoscale sensitivity. The detailed theory of the nsOCT approach is presented in the ESI.†

To realize nsOCT we first convert the collected complex amplitudes of the spectrum to complex amplitudes of axial spatial frequencies. It can be done by noting that each wavelength defines a unique Ewald sphere cap in *K*-space[4] which is transformed into the point on the axis for a single A-scan. After that we decompose the recorded complex spectrum of axial spatial frequencies into multiple sub-bands. OCT images (A-scans) for each sub-band are reconstructed and each image corresponds to a single sub-band of spatial frequencies or to mean axial spatial frequency (period) within each sub-band. By taking the energy contribution of each sub-band from a given point of each reconstructed image we calculate the spatial period profile for this given image point or for the area of interest. As a result, axial spatial frequency (period) profiles can be reconstructed for each voxel of the 3D image. A submicron local structure can be visualized as corresponding spatial period profiles and nanoscale structural alterations within each voxel can be detected. The signal processing flow chart for conventional FDOCT and nsOCT can be found in the ESI.† In addition to nsOCT the conventional OCT image can be reconstructed. It is important to note that there is a trade-off between the width of sub-bands and the axial size of the voxel of the reconstructed image, with the optimal choice being application specific.[6]

Different informative parameters can be extracted from the local axial spatial period profiles to characterize structures, depending on application, and presented as the nsOCT colour image. For example, one of these parameters can be the dominant spatial frequency (period) which corresponds to the maximum signal magnitude and is directly related to the dominant size of the local structure.

To experimentally demonstrate the capabilities of nsOCT we used a full range spectral domain OCT (SD-OCT) setup. A broadband 1310 nm superluminescent diode with a bandwidth of 83 nm was coupled into an interferometer *via* an optical coupler. The spectrometer setup had a spectral resolution of 0.14 nm. The frame rate for B-scan (depth-lateral coordinates) was 50 Hz. The measured voxel size of the OCT system was $\sim$30 μm × 30 μm × 12 μm in air (x, y, z). The uncertainty in spatial periods' determination for NA = 0.03 was less than 1 nm. The voxel size in nsOCT images was 30 μm × 30 μm × 50 μm and spatial interval to reconstruct profiles of the axial spatial periods was 4 nm.

Firstly, to demonstrate the ability of our approach to probe the axial structure within a highly scattering 3D object with nanoscale sensitivity, we used a sample which consists of two layers of self-assembled aggregates of polystyrene nanospheres of known sizes. Such a sample produces a highly scattering 3D quasi-periodic structure in which the spatial periods depend on the nanosphere size and packing,[4] while also introducing some complexity and can serve as a surrogate tissue phantom. The sample was validated using transmission electron microscopy (TEM) and the corresponding images of the spheres in two layers are presented in Fig. 1a and b. The measured diameters of the nanospheres were 614 ± 18 nm and 644 ± 20 nm (mean + standard deviation), so there was some probability that nanospheres from different layers could have the same diameters. In Fig. 1c and d a top layer contains nanospheres with 614 nm mean diameter and a bottom layer contains nanospheres with 644 nm mean diameter. These layers of nanosphere aggregates, whose sizes are well beyond the resolution limit of the OCT system, are indistinguishable in the conventional depth resolved OCT image Fig. 1c and, of course, the mean difference of 30 nm between them cannot be detected. But the nsOCT approach permits us to visualize such a difference as a difference in corresponding spatial periods. The axial spatial period profiles for two selected points in the bottom layer and for two points in the top layer are shown in Fig. 1c. One can see that the positions of the maximum in the profiles within the bottom layer are shifted to larger spatial periods (larger dominant sizes of the structure) relative to corresponding positions of the

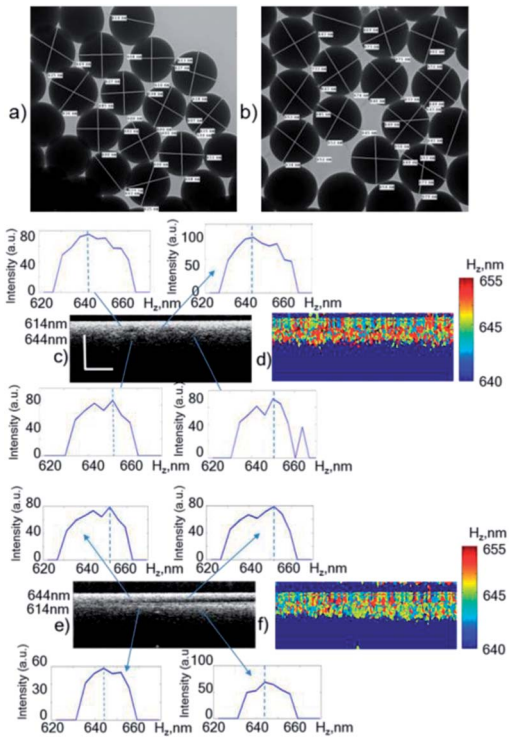

Fig. 1 Images of nanospheres 614 nm and 644 nm diameters; (a and b) TEM images (c and e) conventional OCT images (B-scans) with axial spatial period profiles for selected locations. (d and f) nsOCT images. Lateral and depth scale bars on an OCT image are 0.5 mm.

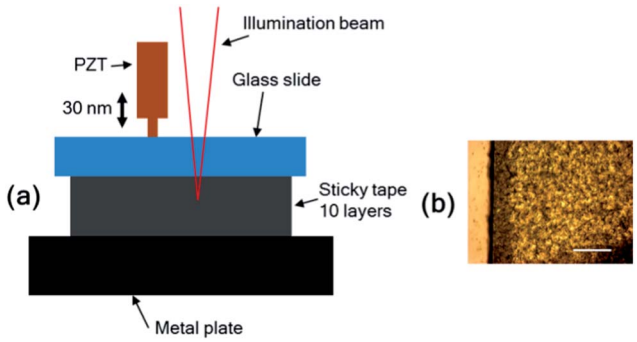

Fig. 2 (a) Schematic of nanoscale structural changes within the sample (multilayer sticky tape); (b) image of the one layer of the tape, scale bar is 200 μm.

maximum in the profiles within the top layer. It means that the structure in the bottom layer has larger dominant size than in the top layer. In Fig. 1d the nsOCT image is shown as a colour map of the dominant axial spatial periods (dominant axial structure sizes). It can be seen that the colours in most locations within the bottom layer are shifted to red relatively to the top layer. It means, according to the colour bar, that the sizes of the axial structure in the bottom layer are larger than the corresponding sizes of the structure in the top layer and it is possible to clearly distinguish two layers with different nanostructures. In Fig. 1e and f the same results are presented when the layers were flipped and the layer with nanospheres of 614 nm mean diameter is in the bottom. These results demonstrate that the difference in structural size as small as 30 nm can be detectable from a single scan using nsOCT (for realization of phase OCT techniques a number of sequential OCT scans are needed,[17,19,24] with severe phase stability and tissue stability requirements).

The ability of nsOCT to detect nanostructural changes within 3D objects from just one OCT scan also makes it very attractive for monitoring the structural changes in time. The second experiment demonstrates the ability of nsOCT to detect nanoscale structural changes in time using just two frames. The sample, which consists of ten layers of scattering sticky tape, was placed on a solid stable base (metal plate), as shown in Fig. 2. We used semi-transparent scotch tape from 3M company (60 μm thick with a mean scattering angle of about 5 degrees), with optical scattering properties very similar to an optical diffuser.[25] The metal plate was rigorously fixed to the bench. A glass slide was placed on top of the sample. The top surface of the sample was shifted 30 nm along the depth direction by a piezoelectric transducer while the bottom surface remained stable. As a result structural changes (deformations) smaller than 30 nm were introduced within the sample. We recorded 50 B-scans before and 50 B-scans after the changes were made. Images in Fig. 3 demonstrate that there are no detectable structural changes at selected locations between the second (Fig. 3a and c) and last (Fig. 3b and d) frames before and after structural changes were made. The profiles of the axial spatial periods in the second (Fig. 3a and c) as well as in the last (Fig. 3b and d) frames remain unchanged.

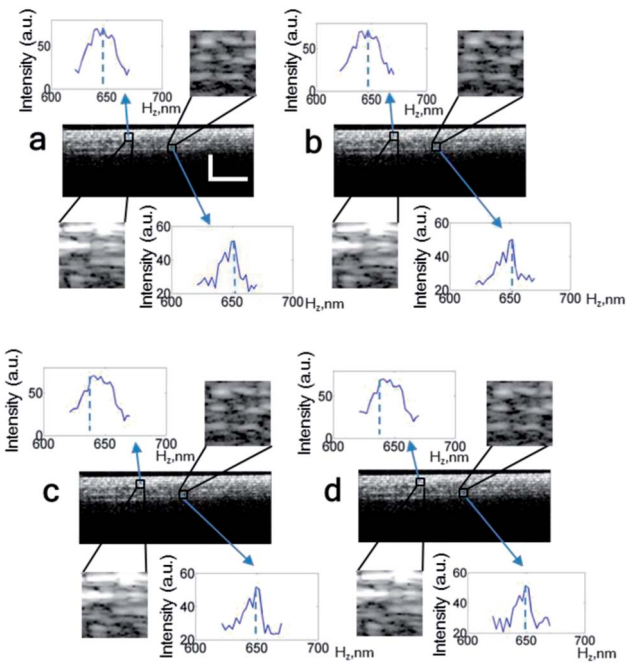

Fig. 3 OCT images of multilayer scattering tape with axial spatial period profiles and magnified portions for the two selected locations. (a and b) before and (c and d) after the top surface displacement of 30 nm. Images (a and c) are second frames and images (b and d) are fiftieth frames. Lateral and depth scale bars are 500 μm.

The dominant spatial periods of the internal structure in corresponding nsOCT images, shown as colour maps in Fig. 4, also remain unchanged for the presented second, last and averaged frames before (Fig. 4a–c) and for corresponding frames (Fig. 4d–f) after the changes were made. These results confirm that the system was stable; the standard deviations of the maximal spatial periods for selected points were 10^{-13} nm and 1.18 nm before and 10^{-13} nm for both locations after structural changes.

It is impossible to get any information about nanostructural changes by comparing conventional OCT images before (Fig. 3a and b) and after (Fig. 3c and d) structural changes, but these changes can be clearly seen by comparing the profiles of the axial spatial periods (also see Fig. 1 in the ESI†). The maximum spatial periods were decreased by 5.27 nm and 1.69 nm for the two selected locations correspondingly. Such structural changes are visualised in nsOCT images in Fig. 4 as a corresponding colour shift between images Fig. 4a–c and 4d–f and the difference can be clearly seen in the corresponding magnified portions. This experiment confirms that temporal nanoscale structural changes smaller than 30 nm can be detected from 2 frames using nsOCT.

In the next experiment we demonstrate the ability of nsOCT to detect relatively fast structural changes, such as blood flow, within highly scattering media. We imaged Brownian motion within intralipid in plastic tubes with an internal diameter of 300 microns, filled with 9% intralipid, through a scattering medium, seven layers of the same scattering tape that was used in the previous experiment.

The time interval between images Fig. 5a and c and Fig. 5b and d was 20 ms. It can be seen that there are obvious changes in the profiles of the axial spatial periods for points within the tubes, but there are no visible changes for points outside the tubes. The fast changes in the axial structure within the tubes can be seen in Videos 1 and 2† while for points outside the tubes (Videos 3 and 4†) these changes are small and slow, and the dominant spatial period remains almost unchanged. In magnified portions of the nsOCT images in Fig. 5c and d and in Video 5† the structural changes within tubes are clearly seen.

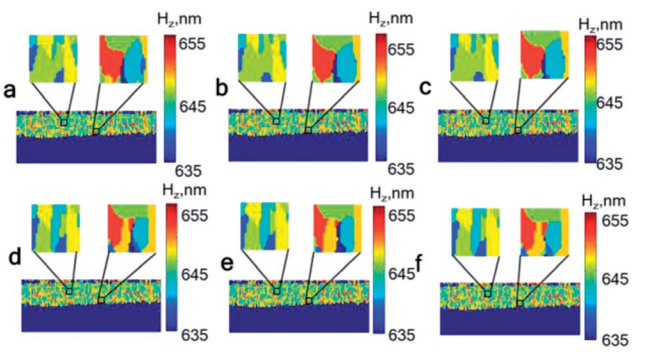

Fig. 4 nsOCT images of multilayer scattering tape with magnified portions for the two selected locations. (a–c) before and (d–f) after the top surface displacement of 30 nm. Images (a and d) are second frames, images (b and e) are fiftieth frames and images (c and f) are averaged images for 49 frames.

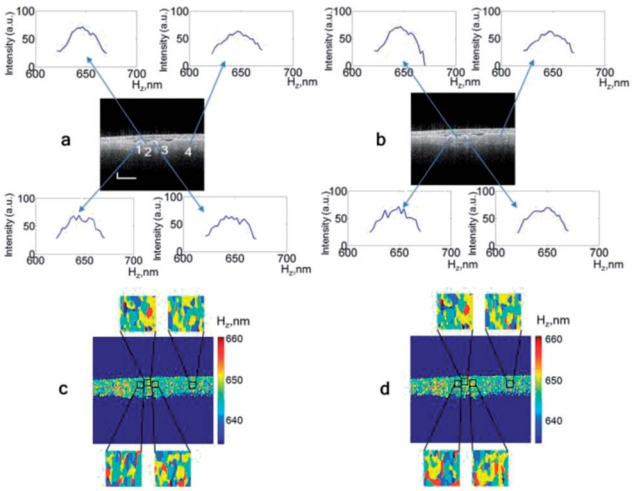

Fig. 5 OCT (a and b) and nsOCT (c and d) images of intralipid within two tubes. For the two selected locations within the tubes and two locations outside the tubes the profiles of the axial spatial periods and magnified portions of nsOCT images are presented. Lateral and depth scale bars are 500 μm.

Finally, in Fig. 6 an example of nsOCT application to *in vivo* imaging of human skin is presented. Within living tissue there are always nanoscale structural changes, but we found that in some areas within the finger nail fold the alterations in the internal structure are faster than in other areas, similar to the previous experiment. The time interval between images Fig. 6a and c and Fig. 6b and d was also 20 ms. We can see the structural changes in the profiles of the axial spatial periods (Fig. 6a and b) and in the magnified portions of the nsOCT images (Fig. 6c and d) for points 2 and 4 during this time interval, while in other areas (points 1 and 3) the structure remains unchanged. In Videos 7 and 9† the fast structural changes in time at points 2 and 4 are shown while for points 1 and 3 in Videos 6 and 8† the

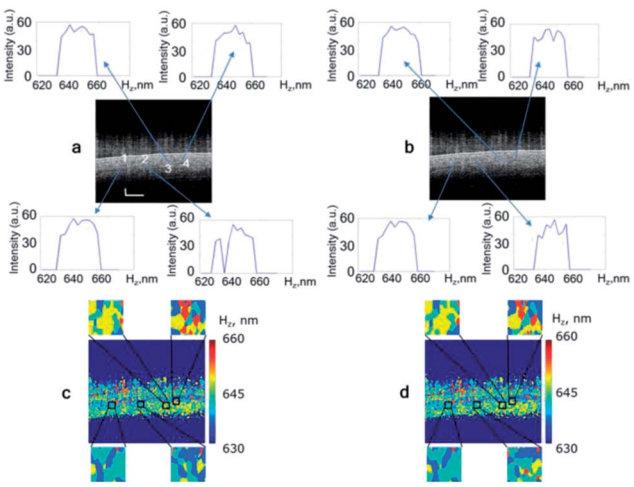

Fig. 6 OCT (a and b) and nsOCT (c and d) *in vivo* images of a finger nail fold. For the four selected locations the axial spatial period profiles and magnified portions of nsOCT images are presented. Lateral and depth scale bars are 500 μm.

corresponding structural changes are relatively slow and small, with a relatively stable dominant spatial period. Video 10† shows nsOCT images of the human nail fold *in vivo* in time where the areas with fast structural changes can be detected. By comparison with results in Fig. 5 and Videos 1–5,† the likely reason for such structural changes is blood flow.

In summary, we have developed a novel technique, nsOCT, to dramatically improve the sensitivity of OCT to structural changes. The application of the SESF principle, which encodes spatial frequency through spectral diversity, results in structural characterization of the scattering object with nanoscale sensitivity. Sensitivity improvement by more than 300 times has been demonstrated; using an OCT system with a resolution 30 μm × 30 μm × 12 μm we were able to detect the size difference between nanosphere aggregates as small as 30 nm from a single OCT scan and temporal structural changes within scattering samples less than 30 nm from just two frames. The nsOCT sensitivity is limited by the spectral resolution, the collected range of spatial frequencies is limited by the spectral range and both can go far beyond what we have demonstrated here. The ability of nsOCT to probe human skin *in vivo* has also been shown and we expect that the technique could be applicable in early detection and treatment of disease.

The authors would like to acknowledge the assistance of Éadaoin Timmins and Pierce Lalor with TEM imaging. The work was supported by the Galway University Foundation, the University of Limerick Foundation, Compact Imaging Inc. and Covidien Inc.

Notes and references

1 S. W. Hell, *Nat. Biotechnol.*, 2003, **21**, 1347–1355.
2 M. G. Gustafsson, *Proc. Natl. Acad. Sci. U. S. A.*, 2005, **102**, 13081–13086.
3 M. Fernandez-Suarez and A. Y. Ting, *Nat. Rev. Mol. Cell Biol.*, 2008, **9**, 929–943.
4 S. A. Alexandrov, S. Uttam, R. K. Bista, K. Staton and Y. Liu, *Appl. Phys. Lett.*, 2012, **101**, 033702.
5 S. A. Alexandrov, S. Uttam, R. K. Bista, C. Q. Zhao and Y. Liu, *Opt. Express*, 2012, **20**, 9203–9214.
6 S. Uttam, S. A. Alexandrov, R. K. Bista and Y. Liu, *Opt. Express*, 2013, **21**, 7488–7504.
7 D. Huang, E. A. Swanson, C. P. Lin, J. S. Schuman, W. G. Stinson, W. Chang, M. R. Hee, T. Flotte, K. Gregory, C. A. Puliafito and J. G. Fujimoto, *Science*, 1991, **254**, 1178–1181.
8 D. C. Adler, Y. Chen, R. Huber, J. Schmitt, J. Connolly and J. G. Fujimoto, *Nat. Photonics*, 2007, **1**, 709–716.
9 L. B. Liu, J. A. Gardecki, S. K. Nadkarni, J. D. Toussaint, Y. Yagi, B. E. Bouma and G. J. Tearney, *Nat. Med.*, 2011, **17**, 1010.
10 B. J. Vakoc, R. M. Lanning, J. A. Tyrrell, T. P. Padera, L. A. Bartlett, T. Stylianopoulos, L. L. Munn, G. J. Tearney, D. Fukumura, R. K. Jain and B. E. Bouma, *Nat. Med.*, 2009, **15**, 1219.
11 R. N. Graf and A. Wax, *Opt. Express*, 2005, **13**, 4693–4698.
12 J. W. Pyhtila and A. Wax, *Opt. Express*, 2004, **12**, 6178–6183.
13 F. Robles, R. N. Graf and A. Wax, *Opt. Express*, 2009, **17**, 6799–6812.
14 K. J. Chalut, J. H. Ostrander, M. G. Giacomelli and A. Wax, *Cancer Res.*, 2009, **69**, 1199–1204.
15 F. E. Robles, C. Wilson, G. Grant and A. Wax, *Nat. Photonics*, 2011, **5**, 744–747.
16 T. S. Ralston, D. L. Marks, P. S. Carney and S. A. Boppart, *Nat. Phys.*, 2007, **3**, 129–134.
17 F. Chen, D. Zha, A. Fridberger, J. Zheng, N. Choudhury, S. L. Jacques, R. K. Wang, X. Shi and A. L. Nuttall, *Nat. Neurosci.*, 2011, **14**, 770–774.
18 H. M. Subhash, N. H. Anh, R. K. K. Wang, S. L. Jacques, N. Choudhury and A. L. Nuttall, *J. Biomed. Opt.*, 2012, **17**, 060505.
19 W. Choi, B. Potsaid, V. Jayaraman, B. Baumann, I. Grulkowski, J. J. Liu, C. D. Lu, A. E. Cable, D. Huang, J. S. Duker and J. G. Fujimoto, *Opt. Lett.*, 2013, **38**, 338–340.
20 J. Yi, A. J. Radosevich, J. D. Rogers, S. C. P. Norris, I. R. Capoglu, A. Taflove and V. Backman, *Opt.Express*, 2013, **21**, 9043–9059.
21 E. Wolf, *Opt. Commun.*, 1969, **1**, 153–156.
22 M. Born and E. Wolf, *Principles of optics: electromagnetic theory of propagation, interference and diffraction of light*, Cambridge University Press, Cambridge, New York, 1999.
23 A. F. Fercher, C. K. Hitzenberger, G. Kamp and S. Y. Elzaiat, *Opt. Commun.*, 1995, **117**, 43–48.
24 R. K. Wang and A. L. Nuttall, *J. Biomed. Opt.*, 2010, **15**, 056005.
25 B. N. J. Persson, A. Kovalev, M. Wasem, E. Gnecco and S. N. Gorb, *EPL*, 2010, **92**, 46001.